Bacteriochlorophyll Aggregates Self-Assembled on Functionalized Gold Nanorod Cores as Mimics of Photosynthetic Chlorosomal Antennae: A Single Molecule Study

Shu Furumaki,[†] Frantisek Vacha,[‡] Shuzo Hirata,[†] and Martin Vacha*[,†]

[†]Department of Organic and Polymeric Materials, Tokyo Institute of Technology, Ookayama 2-12-1-S8, Meguro-ku, Tokyo 152-8552, Japan, and [‡]Institute of Physical Biology, University of South Bohemia and Institute of Plant Molecular Biology, Academy of Sciences of the Czech Republic, Branisovska 31, Ceske Budejovice 370 05, Czech Republic

ABSTRACT We prepare artificial aggregates that mimic the structure and function of natural chlorosomal light harvesting complexes of green photosynthetic bacteria. Gold nanorods functionalized with hydroxyl groups and immobilized on a substrate serve as cores for the growth of bacteriochlorophyll (BChl) aggregates from a buffer solution. The BChl pigments form large self-assembled aggregate particles with sizes more than twice that of natural chlorosomes. The size is controllable by the aggregation time. The aggregates are characterized on a single-particle level by atomic force microscopy, electron microscopy, and single-molecule spectroscopy. The absorption and fluorescence spectral properties which reflect the molecular level arrangement of the BChl aggregates closely resemble those of the natural chlorosomes of the photosynthetic bacterium *Chlorobaculum tepidum*. On the other hand, the results of linear dichroism and circular dichroism are different from those of the chlorosomes and indicate a different mesoscopic structure for the artificial aggregates. These results emphasize the structural role played by the baseplate pigment—protein complex in natural chlorosomes.

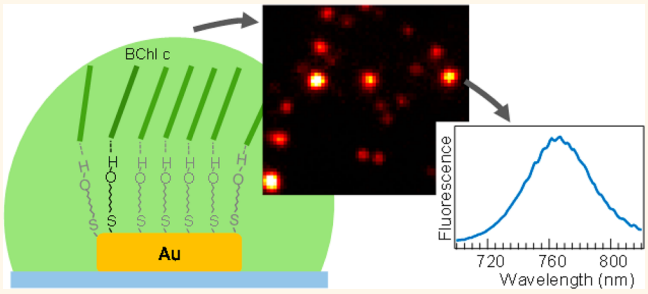

KEYWORDS: single molecule spectroscopy · molecular aggregate · bacteriochlorophyll · chlorosome · gold nanorod · light-harvesting

Chlorosomes are large light-harvesting complexes of green bacteria[1,2] containing mainly bacteriochlorophyll (BChl) *c*, *d*, or *e* molecules which are assembled into large aggregates.[3−5] The aggregates are held together by a combination of hydrogen bonds, coordination bonds, and $\pi-\pi$ interactions.[6] The strong excitonic coupling in the J-type aggregates leads to large red shift of the BChl absorption and fluorescence spectra. Up to 200 000 aggregated BChl molecules are contained in an envelope of lipid monolayer and proteins. The ovoid-shape structures typically have dimensions up to ~180 nm × 60 nm × 30 nm. The large number of BChl molecules and the structure and size of the aggregates enable the green bacteria to capture and utilize incident light with very high efficiency over a broad spectral range which stretches to the near-infrared (NIR) part of the spectrum. As such, chlorosomes serve as ideal models for energy conversion systems and could be an inspiration for, *e.g.*, artificial light harvesting complexes in organic photovoltaic devices where they would help utilize the light energy in the NIR region.

There has been continued interest in artificially replicating the structure and function of photosynthetic antennae including chlorosomes.[7−16] Aggregates of natural BChl molecules and their synthetic counterparts form in aqueous solutions as

* Address correspondence to vacha.m.aa@m.titech.ac.jp.

Received for review October 2, 2013 and accepted February 21, 2014.

Published online February 21, 2014
10.1021/nn500224v

well as in nonpolar organic solutions. Apart from BChl, natural chlorosomes contain significant amounts of carotenes. The presence of lipophilic substances such as carotenoids is crucial for the growth of artificial aggregates of BChl in polar solvents. It has been shown that the aggregation in the polar aqueous solutions is promoted by the addition of nonpolar compounds such as lipids[17] or carotenoids.[18] The spontaneously formed aggregates are spectroscopically very similar to the natural chlorosomes. Structurally, they often form nanorods[11−16] which can range in diameter from a few to tens of nanometers and can be up to a few micrometers long. In natural chlorosomes a pigment−protein structural unit of the envelope called a baseplate plays an indispensable although not fully understood role in the formation of the BChl aggregates.[19]

In this paper, we aim to prepare artificial aggregates that would mimic natural chlorosomes both structurally and functionally. In an attempt to emulate partially the role of the baseplate in the growth of the aggregates we used functionalized gold nanorods that are 50 nm in length and 10 nm in width as cores of the aggregates. The nanorods are immobilized on a substrate, and aggregates of BChl *c* which form on the nanorods are studied on a single particle level by microscopic methods. The aggregation of BChl pigments is initiated by the presence of hydroxyl groups on the gold surface which can form hydrogen bonds with the carbonyl groups on the BChl. The coaggregation of BChl with carotenoids from aqueous buffer solution leads to the formation of large aggregate particles with sizes more than twice that of natural chlorosomes. The size is controllable by the aggregation time. The spectral properties of the aggregates closely resemble those of the natural chlorosomes of the photosynthetic bacterium *Chlorobaculum tepidum*.

RESULTS AND DISCUSSION

The BChl aggregates were prepared mainly on gold nanorods functionalized with 9-mercapto-1-nonanol (C9) linkers, and these aggregates were also fully structurally and spectroscopically characterized. The shorter 3-mercapto-1-propanol (C3) linkers were used as a reference to study the effect of exciton-plasmon interaction in the aggregates. The results obtained on the aggregates were also compared with natural chlorosomes of the photosynthetic bacterium *Chlorobaculum tepidum*.

A typical atomic force microscopy (AFM) image of the BChl aggregates self-assembled on nanorods functionalized with the C9 linker (BChl-C9) and grown for 24 h is shown in Figure 1a. The images show structures with irregular shapes and different sizes dispersed on the surface. To obtain information on the aggregate size, 58 particles were individually scanned and their

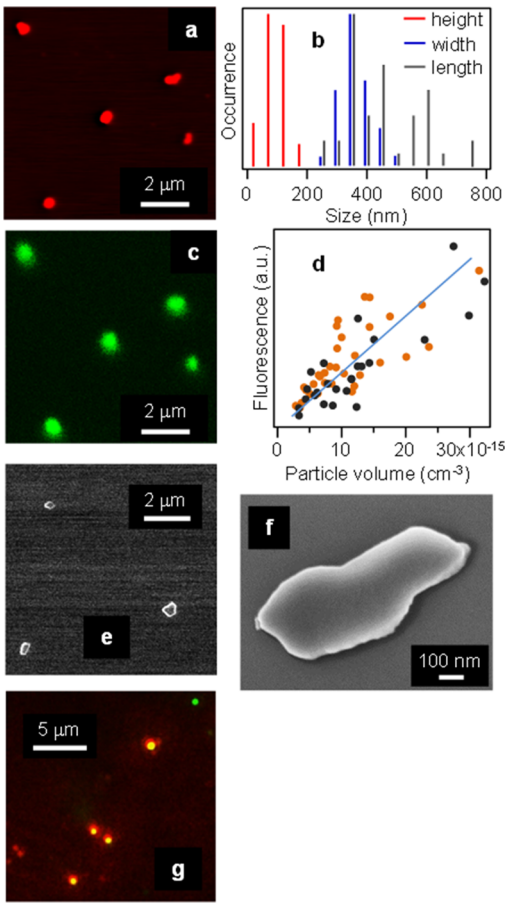

Figure 1. (a) Atomic force microscopy image (AFM) of BChl-C9 aggregates immobilized on a glass surface. (b) Histogram of sizes of BChl-C9 aggregates obtained from the AFM images. (c) Scanning confocal fluorescence image of BChl-C9 aggregates. The image is taken from the same place of the sample as the AFM image shown in (a). (d) Correlation between fluorescence intensity and aggregate particle volume for BChl-C9 aggregates (black) and BChl-C3 aggregates (orange). (e) Field emission scanning electron microscopy (FESEM) image of BChl-C9 aggregates. (f) Detailed FESEM image of an individual BChl-C9 aggregate particle. (g) Composite image of dark field scattering from bare gold nanorods (green) and fluorescence from BChl aggregates (red). Overlap of the gold nanorods and BChl aggregates appears as yellow.

length, width, and height were analyzed. The data are summarized in a histogram in Figure 1b. The average size parameters obtained as means of the distributions were 500 nm for the length, 400 nm for the width, and 110 nm for the height. Figure 1c shows a confocal fluorescence image taken simultaneously with the AFM image. The fluorescence is excited at 488 nm and detected above 750 nm. There is a one-to-one correspondence between the images, indicating that the objects observed in the AFM image emit fluorescence in the spectral region corresponding to aggregates of BChl *c*. Moreover, there is an apparent relation between the particle size and fluorescence intensity between the images. This correlation is confirmed in Figure 1d in which fluorescence intensity is plotted as a function of the particle volume (calculated from the

size parameters assuming an ovoid shape). There is a linear correlation between the intensity and particle volume for both BChl-C9 (black) and BChl-C3 (orange) aggregates.

The shapes and sizes of individual aggregates were also checked using field-emission scanning electron microscopy (FESEM). The results, examples of which are shown in Figure 1e,f, correspond well with the AFM measurements and provide further details on the aggregate morphology. On average, both BChl-C9 and BChl-C3 grow to similar sizes and their volume is about 2 orders of magnitude larger than that of natural chlorosomes. Apart from a different volume, the aspect ratio (length-to-width) of the BChl aggregates of ~1.25 is much smaller than the ratio of ~3 for the chlorosomes.

To directly verify that the BChl aggregates grow on the gold nanorod cores, we carried out an experiment in which we first imaged the gold nanorods deposited on the glass using dark field microscopy before the addition of the BChl. After that, we grew the BChl aggregates without moving the sample from the microscope stage and imaged the BChl aggregates in fluorescence in the same sample area. An example of the results is shown in Figure 1g where the green color represents dark field scattering from the nanorods, the red color represents the fluorescence from the BChl aggregates, and the overlap of the two appears as yellow spots. From these experiments we conclude that more than 70% of the nanorods are covered with the aggregates. To further examine the effect of the gold nanorods on the aggregate growth we prepared a control sample on a bare cover glass. Other experimental conditions (including the functionalization step *via* the thiol coupling carried out on the bare glass) were identical to the BChl-C9 preparation for 24 h. As seen from Figure S1, BChl aggregates do form even without the presence of gold nanorods. However, their density (observed as density of the fluorescence spots in the microscopic image) is much smaller and their average size deduced from the average fluorescence intensity is only about 3% of that of the BChl-C9 aggregates. We may thus conclude that the functionalized gold nanorods are crucial for the initiation and growth of the BChl aggregates.

We characterized the growth of the BChl-C9 aggregates by continuously measuring the microscopic fluorescence images and spectra of the same aggregates during the time that the functionalized nanorods dispersed on the cover glass were covered with the pigment buffer solution (aggregation time), that is, between 3.5 and 24 h. Examples of the fluorescence spectra (normalized) are shown in Figure 2a. For the shortest amount of time of 3.5 h, the spectrum shows a peak at ~670 nm due to the monomeric BChl in the solution and a peak at ~760 nm due to the BChl aggregate (see below). With increasing time, the

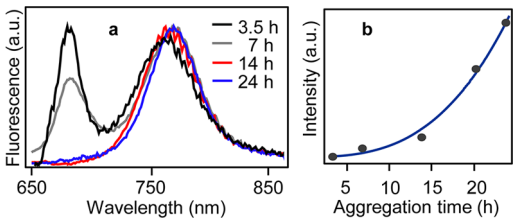

Figure 2. (a) Fluorescence spectra of BChl-C9 aggregate taken at different times during the aggregate growth. (b) Fluorescence intensity analyzed from the long-wavelength band in (a) as a function of the aggregation time, fitted with a third power function.

monomeric peak decreases in intensity and eventually disappears because the size of the aggregate becomes comparable with the optical resolution of the microscope and the fluorescence from the pigment solution is overwhelmed by the aggregate fluorescence at the particle location. At the same time the aggregate peak shifts slightly from 760 to 772 nm. An example of fluorescence intensity from a single aggregate analyzed from the long-wavelength peak of the fluorescence spectra is plotted in Figure 2b as a function of the aggregation time.

Taking into account that the intensity is proportional to the particle volume (as seen in Figure 1d), assuming that the aggregates grow at a constant rate during the 24 h and assuming further that the growth is isotropic (growth in any dimension is linearly proportional to time), the intensity (approximate volume) should be a third power function of the time (approximate dimension). The third power fit to the data points in Figure 2b fits the experimental results reasonably well.

The results of single-molecule characterization and spectroscopy are presented in Figure 3. We note that the characterization was carried out on the largest aggregates grown for 24 h because some of the microscopic methods such as direct absorption of individual particles and, especially, circular dichroism are very sensitive to the total signal and the signal-to-noise ratio and, generally, larger particles provide more reliable data. Similar to individual chlorosomes,[20] single BChl-C9 particles are detected in microscopic transmission images taken with a halogen lamp and a 740 nm band-pass filter. An example of the transmission image is shown in Figure 3a. The transmission data were analyzed by carefully determining the average I_0 base level (100% transmission) in the vicinity of each particle individually and using the value together with the peak transmission intensity I_T to calculate the optical density. The average optical density was 0.35. This value is an order of magnitude larger than that obtained on natural chlorosomes and is very large for a subwavelength size object. The absorption spectrum of the BChl-C9 aggregates is shown in Figure 3b. Since we do not have means to measure the absorption

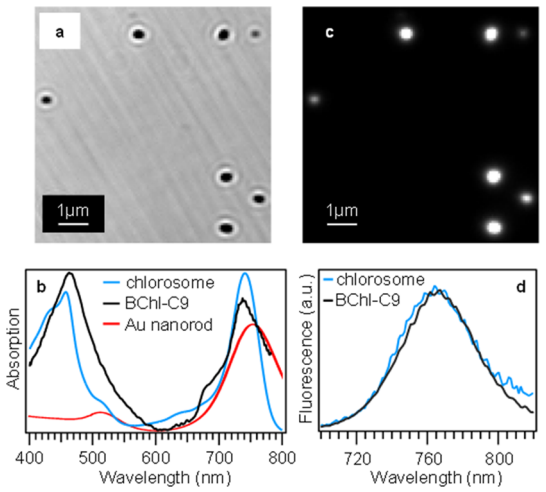

Figure 3. (a) Transmission microscopic image obtained with a halogen lamp and 740 nm bandpass filter. (b) Ensemble absorption spectrum of BChl-C9 aggregates immobilized on a surface (black), together with an absorption spectrum in solution of chlorosomes of *C. tepidum* (blue) and extinction spectrum in solution of gold nanorods (red). (c) Fluorescence microscopic image of the same sample area as in a). (d) Examples of fluorescence spectra of a single BChl-C9 aggregate (black) and a single chlorosome (blue) excited with 457 nm.

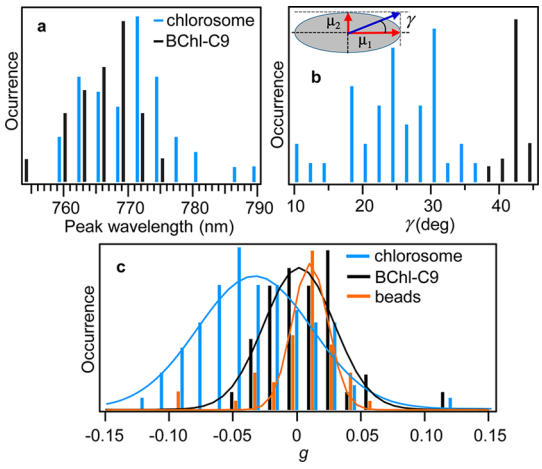

Figure 4. (a) Distribution of fluorescence spectral peaks of BChl-C9 aggregates (black) and chlorosomes (blue). (b) Distribution of the linear dichroism parameter γ (defined in the inset where μ_1 and μ_2 are overall transition dipole moments) for the BChl-C9 aggregates (black) and chlorosomes (blue). (c) Distribution of the circular dichroism dissymmetry parameter *g* for the BChl-C9 aggregates (black), chlorosomes (blue), and fluorescent beads (orange), fitted with Gaussian functions.

spectra of individual particles under the microscope, the spectrum corresponds to an ensemble of BChl-C9 particles on the substrate. The peak at 738 nm is red-shifted from the absorption of monomeric BChl *c* (with peak at 670 nm in methanol) and indicates formation of strongly coupled J-aggregates of BChl *c*. The shoulder around 680 nm could correspond to remaining monomeric BChl *c* or to lower aggregates. Similar absorption spectra have been reported for BChl *c*/carotenoid aggregates in solution.[10] For comparison, Figure 3b also shows the absorption of isolated chlorosomes of *C. tepidum* in buffer solution with a long-wavelength peak of 740 nm. The extinction spectra of the suspension of gold nanorods (also in the Figure 3b) have peaks around 515 and 755 nm, corresponding to the transversal and longitudinal localized plasmon resonances.

A fluorescence image of the same area of the sample as that of the transmission image is shown in Figure 3c. There is a full correspondence between the transmission and fluorescence images, and a correlation can be seen between the transmittance of individual particles and their fluorescence intensity. An example of a fluorescence spectrum taken from a single BChl-C9 particle is shown in Figure 3d, together with a spectrum from a single chlorosome.

A distribution of fluorescence spectral peaks obtained by Gaussian fitting of the spectra of 25 particles is shown in the histogram in Figure 4a, together with a distribution taken from the natural chlorosomes. The mean of the BChl-C9 distribution is 768 nm, comparable to the mean of 772 nm for the chlorosomes. The origin of the fluorescence peak distribution can be related to a large amount of structural disorder present in all aggregates, as mentioned below. Fluorescence is a final step of a complex process that involves absorption, energy transfer, and trapping of the excitation on low-energy sites. The energy of these sites may differ from aggregate to aggregate due to structural differences or differences in the plasmon coupling. We also carried out control experiments to examine the role of the β-carotene in the aggregation process. BChl-C9 aggregates grown for 24 h without the addition of β-carotene show on average much weaker fluorescence intensity and a fluorescence peak shifted to ~750 nm (Figure S2) indicating a smaller aggregate size and lower degree of J-aggregation.

LD (linear dichroism) experiments on single particles of BChl-C9 aggregates are summarized in Figure 4b. The LD has been measured by monitoring fluorescence intensity changes for rotating polarization of the excitation laser (733 nm), after verifying that the fluorescence monitored LD provides the same results as LD directly measured in absorption. The LD has been analyzed in terms of the angle γ between two orthogonal overall transition dipole moments of the particle (see inset of Figure 4b); an isotropic object has $\gamma = 45°$, while complete anisotropy is characterized by $\gamma = 0°$. This parameter has been chosen to facilitate the comparison with previously reported LD results on natural chlorosomes.[20] The mean γ for the chlorosomes is 26°. Compared to this value, the BChl-C9 particles have a mean γ value of 43° and the BChl-C3 particles have a value of 36°. Both BChl-C9 and BChl-C3 show a much lower anisotropy which reflects a less ordered inner structure but could be also affected by

the different aspect ratios for the chlorosomes and the BChl aggregates as observed from the AFM measurements. The large distribution of the parameter γ obtained for the natural chlorosomes reflects the fact that there are large differences in the structural disorder between individual chlorosomes. Chlorosomes with low disorder are characterized by low values of γ, and those with large structural disorder by large γ. Compared to this, BChl aggregates are all disordered to a larger extent, and the extent of the disorder is similar in all aggregates, giving rise to the seemingly narrow distribution of the parameter γ. We note that other studies have found a uniform amount of disorder even on natural chlorosomes.[26]

The difference between the LD of the BChl-C9 and BChl-C3 aggregates could be attributed to the stronger exciton-plasmon coupling in the BChl-C3 particles because of the smaller distance between the innermost pigment layer and the nanorod surface. The good spectral overlap between the nanorod longitudinal plasmon and the aggregate exciton (Figure 3b) would lead to enhanced absorption along the nanorod long axis and larger absorption anisotropy. The stronger exciton-plasmon interaction is also observed by stronger fluorescence quenching in the BChl-C3 particles. The fluorescence intensity of BChl-C3 particles is on average 30% of that of BChl-C9 particles of comparable average volume.

Natural chlorosomes show strong CD that is observable even on the single particle level, with an average CD dissymmetry parameter g of -0.025.[21] The parameter is defined as $g = 2(I_L - I_R)/(I_L + I_R)$ where I_L and I_R are fluorescence intensities excited with left- and right-handed circularly polarized light, respectively. Using the same methodology as in ref 21 we measured CD from individual BChl-C9 aggregates and as a reference from fluorescence beads emitting in the same spectral region and with comparable intensity. The results are shown in Figure 4c. Both BChl-C9 and the fluorescence beads show a Gaussian distribution of the g values, with distribution means of 0.012 for BChl-C9 and 0.009 for the beads. Since the sensitivity of the microscopic CD setup is on the order of 0.005,[21] the observed difference between the aggregates and the beads is within experimental error and may be attributed to the lower fluorescence intensity of the aggregates. Thus, the BChl-C9 aggregates do not show any appreciable circular dichroism. For a reference, Figure 4c also shows a distribution of the g values for single chlorosomes as measured in ref 21, with an apparent shift of the distribution peak and a much larger width due to structural variations between the individual chlorosomes.

Absorption and fluorescence spectra of molecular aggregates reflect the excitonic coupling between individual monomers as well as the size of the aggregate and are affected by the amount of disorder.[22−24] From the similarity between the spectral positions and widths of absorption and fluorescence of natural chlorosomes and the BChl-C9 aggregates (Figure 3b,d, Figure 4a), we can conclude that the aggregation state of BChl-C9 on the molecular level is similar to that of chlorosomes of *C. tepidum*. On the other hand, LD and CD spectra reveal the mesoscopic structure of the aggregates. In natural chlorosomes, the two-dimensional BChl aggregates form curved lamellae[3] which can further roll up to form completely enclosed cylinders.[4,5] These higher structures are mainly aligned along the long axis of the chlorosomes which results in strong absorption anisotropy and LD on the single chlorosome level.[20,25,26] Further, the curvature of the lamellae and of the cylinders gives rise to a strong CD signal.[27] The fact that we have not observed a significant LD and CD signal for the BChl-C9 particles indicates that the mesoscopic arrangement of the BChl aggregates is different from that of the chlorosomes. One of the reasons can be the lower size aspect ratio for BChl-C9 (1.25 compared with 3 for the chlorosomes) which alone could explain the observed change in the LD parameters. However, the lack of the CD signal points either to the lack of curved structures or to random curvatures which would cause cancelation of the CD. In any case, while at the molecular level the BChl-C9 aggregates resemble the natural chlorosomes, the mesoscopic structure is significantly different. This is despite the fact that the BChl-C9 aggregates grow on gold nanorod cores with a high aspect ratio of $\sim$5 and that the growth is initiated by hydrogen bonding which is one of the interactions present in the natural chlorosome aggregates.

CONCLUSIONS

In conclusion, we attempted to prepare and characterize 'artificial chlorosomes', bacteriochlorophyll aggregates that would structurally and functionally mimic natural chlorosomal antennae of green photosynthetic bacteria. To emulate the role of the baseplate present in the envelope of natural chlorosomes we used gold nanorods functionalized with hydroxyl groups that would form hydrogen bonds with carbonyl groups of the BChls and initiate the growth of the aggregates. The resulting aggregates form irregular-shape particles that are larger than chlorosomes but in terms of spectroscopic properties are very similar. The mesoscopic structure of the artificial aggregates is different from chlorosomes, pointing to the indispensable role of the baseplate and probably the lipid−protein envelope in the structural growth of natural chlorosomes.

An interesting but unexplored aspect of the present aggregate particles is the good overlap between the exciton band of the BChl aggregates and the plasmon band of the nanorods. The strong interaction between the two could be potentially used to convert the excitons into plasmons, and these could be further

utilized in other energy conversion schemes.[28] The advantage of a molecular aggregate compared to a bare gold nanorod is in the broader spectral range over which the light energy can be efficiently captured.

METHODS

Cells of photosynthetic bacterium *Chlorobaculum tepidum* were grown for 3 days at 48 °C in modified Pfennig's medium[29] under constant illumination and stored at 4 °C until use. Bacteriochlorophyll *c* (BChl *c*) was extracted from pelleted cells by an acetone−methanol mixture in the dark on ice and separated by centrifugation and reversed phase HPLC.[10] The four main homologues of BChl *c* were collected together, dried, and kept under an inert atmosphere at −70 °C until further use.

Gold nanorods (average size 50 nm × 10 nm, size distribution ±10%, surface stabilized with CTAB), β-carotene, 3-mercapto-1-propanol (C3), and 9-mercapto-1-nonanol (C9) were all purchased from Aldrich and used as supplied. To immobilize the gold nanorods on a substrate, the nanorod suspension was diluted 5 times with ultrapure water and 150 μL of the diluted suspension were spin-coated at 3000 rpm on a cleaned microscope cover glass (Thermo Fisher). The immobilized nanorods were functionalized by immersing the cover glass in a 10 mM chloroform solution of either C3 or C9 for 12 h. The cover glass was then rinsed with dichloromethane, acetone, and ultrapure water. In the resulting sample, the functionalized gold nanorods are dispersed without aggregation on the glass surface with a density that allowed individual nanorods to be distinguished with optical resolution (Supporting Information (SI), Figure S3).

To grow the BChl aggregates, a small amount (approximately 1 mg) of BChl *c* was dissolved in 10 μL of methanol and this solution together with 8 μL of a 1.35 mM THF solution of β-carotene was added into 5 mL of 50 mM Tris buffer. 300 μL of the mixture were then placed on top of the cover glass with the functionalized nanorods and left standing for 3.5−24 h to enable the growth of the aggregates. After that, the excess mixture was rinsed with pure 50 mM Tris buffer and the samples were used immediately for experiments. Control samples were also prepared without the gold nanorods on a cleaned cover glass.

The resulting aggregates have been characterized by simultaneous atomic force microscopy (AFM) and confocal fluorescence microscopy, by electron microscopy and by single-molecule fluorescence, absorption, linear dichroism (LD), and circular dichroism (CD) spectroscopy. These methods have been described previously.[20,21,30] Briefly, the AFM head (Asylum Research MPF-3D) is placed on top of a home-built confocal microscope for simultaneous AFM−fluorescence microscopy. Topological images were taken with an uncoated silicon probe (Olympus AC200TS) in the tapping (AC) mode. Fluorescence was collected with an oil-immersion objective lens (100×, NA 1.3) and detected with an avalanche photodiode. Electron microscopy images were taken with a field emission scanning electron microscope (FESEM, JEOL JSM-7401F) at room temperature. The single-molecule spectroscopy experiments were carried out using an inverted fluorescence microscope (Olympus IX-71) with a 457 or 733 nm excitation laser, an electron-multiplication (EM) CCD camera (Andor iXon+), and an imaging spectrograph (Bunkou Keiki CLP-50). All single-molecule experiments were carried out in air at room temperature.

Conflict of Interest: The authors declare no competing financial interest.

Acknowledgment. The FESEM experiments were performed by Dr. J. Nebesarova, Dr. K. Totani, and Y. Takahashi who are gratefully acknowledged. The research was partly supported by the Academy for Co-creative Education of Environment and Energy Science program at the Tokyo Institute of Technology.

Supporting Information Available: Reference experiment without Au nanorods; reference experiment without β-carotene; FESEM images of Au nanorods dispersed on cover glass. This material is available free of charge *via* the Internet at http://pubs.acs.org.

REFERENCES AND NOTES

1. Blankenship, R. E.; Matsuura, K. Antenna Complexes from Green Photosynthetic Bacteria. In *Light-Harvesting Antennas*; Green, B. R., Parson, W. W., Eds.; Kluwer Academic Publishers: Dordrecht, 2003; pp 195−217.
2. Frigaard, N. U.; Bryant, D. A. Chlorosomes: Antenna Organelles in Photosynthetic Green Bacteria. In *Microbiology Monographs*; Shivley, J. M., Ed.; Springer: Berlin, Heidelberg, 2006; Vol. 2, pp 79−114.
3. Psencik, J.; Ikonen, T. P.; Laurinmaki, P.; Merckel, M. C.; Butcher, S. J.; Serimaa, R. E.; Tuma, R. Lamellar Organization of Pigments in Chlorosomes, the Light Harvesting Complexes of Green Photosynthetic Bacteria. *Biophys. J.* **2004**, *87*, 1165–1172.
4. Oostergetel, G. T.; Reus, M.; Gomez Maqueo Chew, A.; Bryant, D. A.; Boekema, E. J.; Holzwarth, A. R. Long-Range Organization of Bacteriochlorophyll in Chlorosomes of Chlorobium Tepidum Investigated by Cryo-Electron Microscopy. *FEBS Lett.* **2007**, *581*, 5435–5439.
5. Ganapathy, S.; Oostergetel, G. T.; Wawrzyniak, P. K.; Reus, M.; Gomez Maqueo Chew, A.; Buda, F.; Boekema, E. J.; Bryant, D. A.; Holzwarth, A. R.; de Groot, H. J. M. Alternating *Syn-Anti* Bacteriochlorophylls Form Concentric Helical Nanotubes in Chlorosomes. *Proc. Natl. Acad. Sci. U.S.A.* **2009**, *106*, 8525–8530.
6. Alster, J.; Kabelac, M.; Tuma, R.; Psencik, J.; Burda, J. Computational Study of Short-Range Interactions in Bacteriochlorophyll Aggregates. *Comp. Theor. Chem.* **2012**, *998*, 87–97.
7. Miyatake, T.; Tamiaki, H. Self-Aggregates of Natural Chlorophylls and their Synthetic Analogues in Aqueous Media for Making Light-Harvesting Systems. *Coord. Chem. Rev.* **2010**, *254*, 2593–2602.
8. Balaban, T. S. Tailoring Porphyrins and Chlorins for Self-Assembly in Biomimetic Artificial Antenna Systems. *Acc. Chem. Res.* **2005**, *38*, 612–623.
9. Balaban, T. S.; Tamiaki, H.; Holzwarth, A. R. Chlorins Programmed for Self-Assembly. *Top. Curr. Chem.* **2005**, *258*, 1–38.
10. Klinger, P.; Arellano, J. B.; Vacha, F.; Hala, J.; Psencik, J. Effect of Carotenoids and Monogalactosyl Diglyceride on Bacteriochlorophyll c Aggregates in Aqueous Buffer: Implications for the Self-assembly of Chlorosomes. *Photochem. Photobiol.* **2004**, *80*, 572–578.
11. Balaban, T. S.; Linke-Schaetzel, M.; Bhise, A. D.; Vanthuyne, N.; Roussel, C.; Anson, C. A.; Buth, G.; Eichhcfer, A.; Foster, K.; Garab, G.; *et al.* Structural Characterization of Artificial Self-Assembling Porphyrins that Mimic the Natural Chlorosomal Bacteriochlorophylls c, d, and e. *Chem.—Eur. J.* **2005**, *11*, 2267–2275.
12. Chappaz-Gillot, C.; Marek, P. L.; Blaive, B. J.; Canard, G.; Burck, J.; Garab, G.; Hahn, H.; Javorfi, T.; Kelemen, L.; Krupke, R.; *et al.* Anisotropic Organization and Microscopic Manipulation of Self-Assembling Synthetic Porphyrin Microrods That Mimic Chlorosomes: Bacterial Light-Harvesting Systems. *J. Am. Chem. Soc.* **2012**, *134*, 944–954.
13. Shoji, S.; Hashishin, T.; Tamiaki, H. Construction of Chlorosomal Rod Self-Aggregates in the Solid State on Any Substrates from Synthetic Chlorophyll Derivatives Possessing an Oligomethylene Chain at the 17-Propionate Residue. *Chem.—Eur. J.* **2012**, *18*, 13331–13341.
14. Huber, V.; Katterle, M.; Lysetska, M.; Wurthner, F. Reversible Self-Organization of Semisynthetic Zinc Chlorins into Well-Defined Rod Antennae. *Angew. Chem., Int. Ed.* **2005**, *44*, 3147–3151.
15. Sengupta, S.; Ebeling, D.; Patwardhan, S.; Zhang, X.; von Berlepsch, H.; Bottcher, C.; Stepanenko, V.; Uemura, S.; Hentschel, C.; Fuchs, H.; *et al.* Biosupramolecular Nanowires

from Chlorophyll Dyes with Exceptional Charge-Transport Properties. *Angew. Chem., Int. Ed.* **2012**, *51*, 6378–6382.
16. Eisele, D. M.; Cone, C. W.; Bloemsma, E. A.; Vlaming, S. M.; van der Kwaak, C. G. F.; Silbey, R. J.; Bawendi, M. G.; Knoester, J.; Rabe, J. P.; Vanden Bout, D. A. Utilizing Redox-Chemistry to Elucidate the Nature of Exciton Transitions in Supramolecular Dye Nanotubes. *Nat. Chem.* **2012**, *4*, 655–662.
17. Uehara, K.; Mimuro, M.; Ozaki, Y.; Olson, J. M. The Formation and Characterization of the *In Vitro* Polymeric Aggregates of Bacteriochlorophyll c Homologs from *Chlorobium limicola* in Aqueous Suspension in the Presence of Monogalactosyl Diglyceride. *Photosynth. Res.* **1994**, *41*, 235–243.
18. Alster, J.; Polivka, T.; Arellano, J. B.; Chabera, P.; Vacha, F.; Psencik, J. β-Carotene to Bacteriochlorophyll c Energy Transfer in Self-Assembled Aggregates Mimicking Chlorosomes. *Chem. Phys.* **2010**, *373*, 90–97.
19. Pedersen, M. O.; Linnanto, J.; Frigaard, N. U.; Nielsen, N. C.; Miller, M. A Model of the Protein−Pigment Baseplate Complex in Chlorosomes of Photosynthetic Green Bacteria. *Photosynth. Res.* **2010**, *104*, 233–243.
20. Furumaki, S.; Vacha, F.; Habuchi, S.; Tsukatani, Y.; Bryant, D. A.; Vacha, M. Absorption Linear Dichroism Measured Directly on a Single Light-Harvesting System: The Role of Disorder in Chlorosomes of Green Photosynthetic Bacteria. *J. Am. Chem. Soc.* **2011**, *133*, 6703–6710.
21. Furumaki, S.; Yabiku, Y.; Habuchi, S.; Tsukatani, Y.; Bryant, D. A.; Vacha, M. Circular Dichroism Measured on Single Chlorosomal Light-Harvesting Complexes of Green Photosynthetic Bacteria. *J. Phys. Chem. Lett.* **2012**, *3*, 3545–3549.
22. Prokhorenko, V. I.; Steensgaard, D. B.; Holzwarth, A. R. Exciton Theory for Supramolecular Chlorosomal Aggregates: 1. Aggregate Size Dependence of the Linear Spectra. *Biophys. J.* **2003**, *85*, 3173–3186.
23. Didraga, C.; Knoester, J. Optical Spectra and Localization of Excitons in Inhomogeneous Helical Cylindrical Aggregates. *J. Chem. Phys.* **2004**, *121*, 10687–10698.
24. Linnanto, J. M.; Korppi-Tommola, J. E. I. Investigation on Chlorosomal Antenna Geometries: Tube, Lamella and Spiral-Type Self-Aggregates. *Photosynth. Res.* **2008**, *96*, 227–245.
25. Jendrny, M.; Aartsma, T. J.; Köhler, J. Fluorescence Excitation Spectra from Individual Chlorosomes of the Green Sulfur Bacterium *Chlorobaculum tepidum*. *J. Phys. Chem. Lett.* **2012**, *3*, 3745–3750.
26. Tian, Y.; Camacho, R.; Thomsson, D.; Reus, M.; Holzwarth, A. R.; Scheblykin, I. G. Organization of Bacteriochlorophylls in Individual Chlorosomes from *Chlorobaculum tepidum* Studied by 2-Dimensional Polarization Fluorescence Microscopy. *J. Am. Chem. Soc.* **2011**, *133*, 17192–17199.
27. Garab, G.; van Amerongen, H. Linear Dichroism and Circular Dichroism in Photosynthesis Research. *Photosynth. Res.* **2009**, *101*, 135–146.
28. Ueno, K.; Misawa, H. Plasmon-Enhanced Photocurrent Generation and Water Oxidation from Visible to Near-Infrared Wavelengths. *NPG Asia Mater.* **2013**, *5*, e61.
29. Wahlund, T. M.; Woese, C. R.; Castenholz, R. W.; Madigan, M. T. A Thermophilic Green Sulfur Bacterium from New Zealand Hotsprings, *Chlorobium tepidum* Sp. Nov. *Arch. Microbiol.* **1991**, *156*, 81–90.
30. Kobayashi, H.; Hirata, S.; Vacha, M. Mechanical Manipulation of Photophysical Properties of Single Conjugated Polymer Nanoparticles. *J. Phys. Chem. Lett.* **2013**, *4*, 2591–2596.